播種することで，再生型心臓弁葉を作成した。ヒツジの肺動脈弁の一葉を再生医療心臓弁葉と置換したところ，6週後には正常組織と同様の組織が再生し，9週以降は力学特性も正常組織と同等であったと報告している[17]。

脱細胞化マトリックスを用いた先駆例としては，米国CryoLife社によるSynerGraft心臓弁がある。1999年から脱細胞化ブタ大動脈弁の臨床使用を開始し，2001年には世界初の再生型心臓弁と称して欧州で市販を開始した。移植後数ヵ月間で自己細胞が組織内に浸潤し，自己組織化すると報告している[18]が，移植後に破断の生じた例も報告されている。ドイツ・ハノーバー医科大学のHaverichらは，1998年より異種生体弁から動物由来細胞を除去し，代わりにレシピエントの自己血管内皮細胞を播種する動物実験を行い，界面活性剤であるTriron X-100や蛋白分解酵素であるトリプシン溶液を細胞除去に用いている[19]。英国リーズ大学のInghamらは種々の薬液で細胞除去効果を検討し，Sodium Dodecyl Sulfate (SDS)が最も細胞除去に適していると報告している[20]。また，ドイツ・フンボルト大学のKonertzらはヒツジを用いた6ヵ月間の実験で，脱細胞化ブタ肺動脈弁に自己内皮細胞を播種することで弁の変形や石灰化もみられなかったと報告しており，臨床使用も開始している[21]。

我々は2000年から，脱細胞化した生体弁に患者自身の細胞を組み込むテーラーメード心臓弁の開発を開始した。免疫反応の主因を成すドナー由来細胞を除去し，コラーゲン線維や弾性線維などの構造マトリックスからなる脱細胞化Scaffoldに患者の自己細胞を組み込むことで，生体適合性を高めるとともに，自己修復性や成長性を有する代用弁が創製できると期待できる(図3)。このためには，完全な脱細胞化処理法の開発による安全な脱細胞化Scaffoldの開発が重要である。

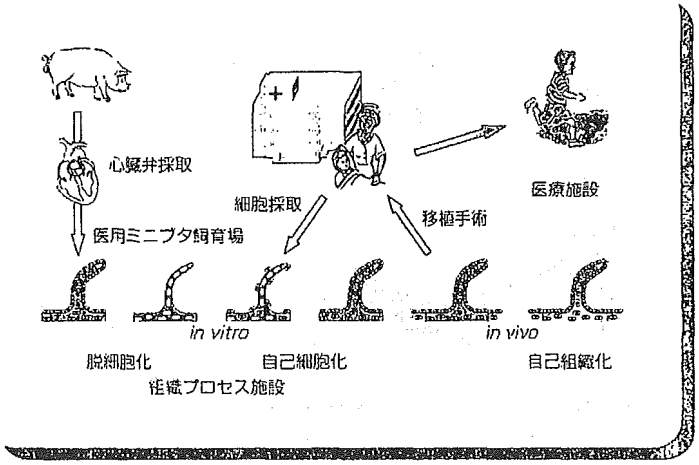

図3　脱細胞化組織を用いた再生医療のスキーム図

3．新規脱細胞化処理

前述のように，ほとんどのグループは界面活性剤や蛋白分解酵素などの薬液処理によって細胞を除去している。我々も当初，Triton X-100溶液による界面活性剤浸漬処理を検討した。その結果，厚さ数百μmの弁葉内においては処理6時間後には細胞核は染色されなくなったが，弁葉基部の組織内細胞の核は処理24時間後でも表面から1mm以遠の組織深部では染色されており，界面活性剤溶液の組織内浸透性が悪いためであると考えられた(図4中)。また，細胞毒性を示すTriton X-100を洗浄除去するために数週間以上の時間を要し，その間における生体力学特性の変化や汚染の危険性についても注意が必要であった。そこで我々は，より完全な細胞除去法について検討し，液体を圧力媒体として等方圧力を加える冷間等方圧加圧法による超高圧印加処理法を開発した(図5)。多くの蛋白質や酵素は300MPa程度の高圧処理によって変性するとともに，酵母や芽胞をもたない細菌は500MPaの処理で細胞膜が破壊され，殺菌される。また，HIVなどのエンベロープをもつウイルスは600MPaの処理でほぼ完全に不活化される[22]。清潔下にて摘出し

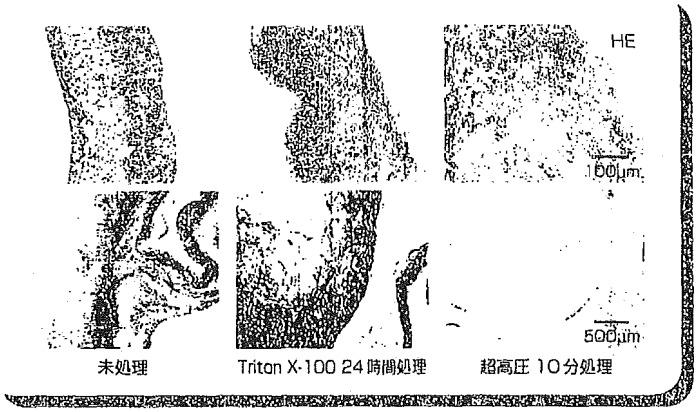

図4　脱細胞化処理された心臓弁の組織断面（上：弁葉，下：弁基部）
（→巻頭Color Gravure参照）

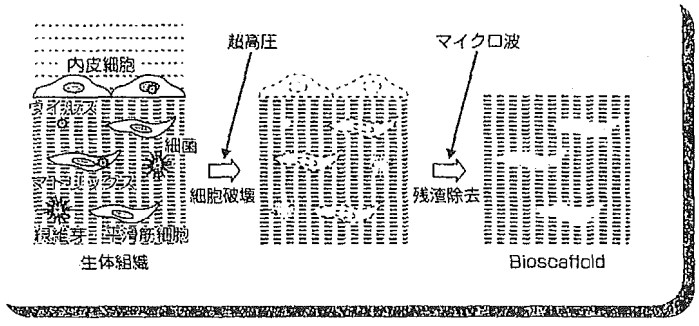

図5　新規な脱細胞処理法

たミニブタ心臓より肺動脈弁を採取し，低温下にて980MPa（10,000気圧）の超高圧印加処理（4℃，10分間）を行い，続いて洗浄処理したところ，組織深部まで完全に細胞を除去することができた（図4右）。力学特性を検討したところ，界面活性剤浸漬処理では，処理時間に伴って強度，弾性率とも増加する傾向を示したが，超高圧処理では力学特性への影響がみられなかった（図6）。現在，超高圧処理および複数種の自己細胞を組み込んだテーラーメード心臓弁の動物実験に取り組んでいる。

再生医療用材料の今後

今後の再生医療に望まれるテクノロジーとしては，①材料・細胞の空間的配置，②時間的制御のための物理刺激法（温度以外の），③成形法および④再生組織の評価があげられる。

①は材料および細胞の空間的配置を制御する技術で，たとえば肝臓や腎臓などでは，働きの異なる細胞が三次元的に階層構造をとっている。このような複雑な構造を工学的な技術で再構築するには，三次元的に細胞を配置するための精緻な加工法とそれに対応した材料開発が必要である。②については，組織再生のカスケードについては，発生学の進展により次第に明らかになってきているが，これによると，種々の蛋白質や遺伝子が時系列順に発現することが明らかになっている。これらの生理的な状況を，再生医療の場で実現するためには，それぞれの因子の作用を時系列的に制御する技術が必要である。一つの手法は，DDSであり，材料の特性を用いたものが考えられる。もう一つの手法は，外部から物理的な刺激によって制御するものである。すでに温度，磁場，超音波などによる薬剤などの放出のOn-Off制御の検討が行われている。今後は全体でなく，空間的な制御法を組み込んだ精緻な位置特異的な放出制御技術の開発が期待される。③については，現在の多孔性もしくは繊維による構築技術だけでなく，細胞の空間配置制御を可能にする

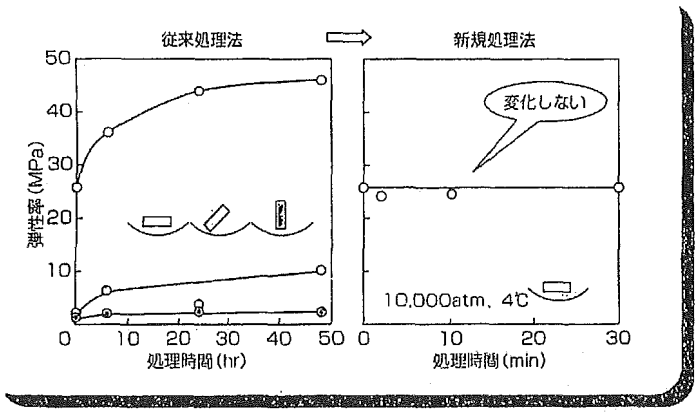

図6　界面活性剤および新規法による脱細胞化弁葉の力学特性評価

ような新しい材料加工法が必要となると思われる。

このように、再生医療における材料の重要性は今後ますます増大していくと思われる。

おわりに

現状の再生医学のための工学技術は、足場材料を含んだバイオマテリアルの開発や細胞を増やすためのバイオリアクターの開発が主体である。発生工学的研究などにより組織再生のメカニズムの全容が明らかになるまでは、材料工学だけでなくすべての工学技術を結集した生体工学技術の発展が、再生医療を支えていくものと思われる。材料研究者と医学研究者の共通する基盤として、再生医療の今後のより一層の発展を祈念する。

謝　辞

共同研究者の木村　剛先生，沼田智先生，庭屋和夫先生，中谷武嗣先生，および北村惣一郎先生の各位に感謝します。また，研究の一部は，厚生労働科学研究費，ヒューマンサイエンス総合研究，循環器病研究委託費事業，および日本学術振興会科学研究費補助金の補助を受けて行われました。

文　献

1) Langer R, Vacanti JP : Tissue engineering. *Science* 260 : 920-926, 1993
2) Shoichet MS, Hubbel JA, eds : Polymers for Tissue Engineering, VSP, Utrecht, 1998
3) de Groot JH, Zijlstra FM, Kuipers HW, et al : Meniscal tissue regeneration in porous 50/50 copoly (L-lactide/epsilon-caprolactone) implants. Biomaterials 18 : 613-622, 1997
4) Giordano GG, Thomson RC, Ishaug SL, et al : Retinal pigment epithelium cells cultured on synthetic biodegradable polymers. *J Biomed Mater Res* 34 : 87-93, 1997
5) DiEdwardo CA, Petrosko P, Acarturk TO, et al : Muscle tissue engineering. Clin Plast Surg 26 : 647-656, 1999
6) den Dunnen WF, Stokroos I, Blaauw EH, et al : Light-microscopic and electron-microscopic evaluation of short-term nerve regeneration using a biodegradable poly (DL-lactide-epsilon-caprolacton) nerve guide. J Biomed Mater Res 31 : 105-115, 1996
7) Kobayashi T, Nakamura S, Yamashita K : Enhanced osteobonding by negative surface charges of electrically polarized hydroxyapatite. J Biomed Mater Res 57 : 477-484, 2001
8) Takahashi Y, Yamamoto M, Tabata Y : Enhanced osteoinduction by controlled release of bone morphogenetic protein-2 from biodegradable sponge composed of gelatin and beta-tricalcium phosphate. Biomaterials 26 : 4856-4865, 2005
9) Omori K, Nakamura T, Kanemaru S, et al : Regenerative medicine of the trachea : the first human case. Ann Otol Rhinol Laryngol 114 : 429-433, 2005
10) Kushibiki T, Nagata-Nakajima N, Sugai M, et al : Delivery of plasmid DNA expressing small interference RNA for TGF-beta type II receptor by cationized gelatin to prevent interstitial renal fibrosis. J Contr Rel 105 : 318-331, 2005
11) Itabashi Y, Miyoshi S, Yuasa S, et al : Analysis of the electrophysiological properties and arrhythmias in directly contacted skeletal and cardiac muscle cell sheets. Cardiovasc Res 67 : 561-570, 2005
12) Kikuchi A, Okano T : Nanostructured designs of biomedical materials : applications of cell sheet engineering to functional regenerative tissues and organs. J

Contr Rel 101 : 69-84, 2005
13) Furuzono T, Yasuda S, Kimura T, et al : Nano-scaled hydroxyapatite/polymer composite IV. Fabrication and cell adhesion properties of a three-dimensional scaffold made of composite material with a silk fibroin substrate to develop a percutaneous device. J Artif Organs 7 : 137-144, 2004
14) Bader A, Schilling T, Teebken OE, et al : Tissue engineering of heart valves—human endothelial cell seeding of detergent acellularized porcine valves. Eur J Cardiothorac Surg 14 : 279-284, 1998
15) Konertz W, Dohmen PM, Liu J, et al : Hemodynamic characteristics of the Matrix P decellularized xenograft for pulmonary valve replacement during the Ross operation. J Heart Valve Dis 14 : 78-81, 2005
16) 日本人工臓器学会レジストリー委員会：人工臓器のレジストリー2000．人工臓器 30 (suppl): 1-8, 2001
17) Shinoka T, Ma PX, Shum-Tim D, et al : Tissue-engineered heart valves : autologous valve leaflet replacement study in a lamb model. Circulation 94 (9 Suppl): II164-168, 1996
18) Elkins RC, Goldstein S, Hewitt CW, et al : Recellularization of heart valve grafts by a process of adaptive remodeling. Semin Thorac Cardiovasc Surg 13 (4 Suppl 1): 87-92, 2001
19) Teebken OE, Puschmann C, Aper T, et al : Tissue-engineered bioprosthetic venous valve : a long-term study in sheep. Eur J Vasc Endovasc Surg 25 : 305-312, 2003
20) Korossis SA, Fisher J, Ingham E : Cardiac valve replacement : a bioengineering approach. Biomed Mater Eng 10 : 83-124, 2000
21) Dohmen PM, Lembcke A, Hotz H, et al : Ross operation with a tissue-engineered heart valve. Ann Thorac Surg 74 : 1438-1442, 2002
22) 鈴木敦士，林　力丸 編：高圧生物科学と高圧技術．さんえい出版，京都，1997

特集「異種移植」

ブタ組織の脱細胞化

菅　理晴[1]，藤里俊哉[1]，永谷憲歳[1]，中谷武嗣[2]
[1]国立循環器病センター再生医療部，[2]同センター臓器移植部

はじめに

一般に組織の置換や欠損部の修復を同種あるいは異種組織移植により行おうとする場合，そのままでは激しい拒絶反応が引き起こされ，組織は壊死・脱落する。この拒絶反応の原因となる同種・異種の主要抗原は主に組織中の細胞膜に存在するため，組織から細胞成分を完全に除去できれば抗原性はほとんど消失すると考えられる。そこで脱細胞化した組織を移植し，これをscaffold（足場）として宿主細胞により組織が再構築されれば，拒絶反応に対する免疫抑制治療の必要なく，場合によっては成長性を期待することもできる新たな再生医療となりえる。

これまで生体組織の脱細胞化法として，急速な凍結・溶解による細胞破壊，界面活性剤や蛋白分解酵素による細胞除去など試みられてきたが，細胞成分の残存，ウィルスを含む病原微生物の存在，組織力学特性の変化，使用薬剤の毒性，組織保存・輸送にかかる費用などの点でそれぞれ一長一短であった。

われわれは，上記諸問題をクリアする脱細胞化方法として新たに超高圧処理法を開発し，各種組織においてその移植可能性を検討しているので，ここにその一部を紹介する。

超高圧処理による脱細胞化

生体組織に液体を圧力媒体として温度上昇を抑えながら等方圧力を加えていくと，多くの機能性蛋白は300 MPa程度の加圧により失活・変性し，酵母や芽胞のない細菌も500 MPaで死滅する。さらに600 MPaではHIVなどのエンベロープを有するウィルスまで不活化させることができる[1]。

そこでわれわれは，低温を保ちながら等方圧力を加えることのできる冷間等方圧印加処理装置（図1）を用い，ブタから採取した各種組織を4℃にて980 MPa（10,000気圧）で10分間加圧し，続いてPBSを主体と

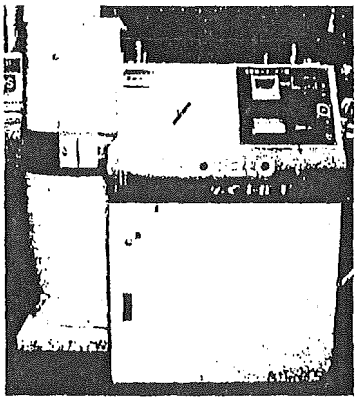

した洗浄液で2週間震盪洗浄した。この処理により，多くの組織では深部まで十分に細胞成分が除去され，その一方でEVG染色においてコラーゲン繊維やエラスチン繊維はそのまま保存されていることが確認された。また，力学試験を行うと力学特性は処理前と同様に保持され，さらにPCR法にてブタ内在性レトロウィルス（PERV）-DNAが検出されなくなっていた。

以上より，本法は異種組織移植を行うための生体scaffold作製法として有望であると考えられた。

心臓弁

脱細胞化異種心臓弁の先駆例としてCryoLife社のSyner Graft心臓弁があり[9]，2001年に欧州で市販された。しかしその成績が必ずしも満足のいくものでなかったこともあり，現在は販売が中止されている。心臓弁の脱細胞化法としてはHaverichらが界面活性剤であるTriton X-100やトリプシンによる方法を[10]，またInghamらがSDSによる細胞除去の有用性を報告している[11]。

われわれも当初Triton X-100溶液を用いた心臓弁の脱細胞化を検討していたが，24時間の浸漬処理と2週間の洗浄を行った後も表層から1 mm程度までしか細胞が除去されず，弁基部の組織内部では大部分の細胞成分が残存した。また，洗浄後も組織中にTriton X-100の残留を認め，力学特性においても弁弾性率が有意に増加したため，最終的にこの方法による脱細胞化処理を中止し，新たな脱細胞化法として超高圧処理法の開発へ移行した。超高圧処理を行った弁では組織深部まで細胞が完全に除去され，力学特性への影響も認めなかった。

心臓弁scaffoldを移植する場合，宿主の自己細胞をあらかじめ移植片に組み込んで移植することで抗血栓性や組織の再構築促進が期待される。われわれはブタ同種心臓弁移植実験において，移植予定の宿主ブタから採取した大腿動脈の血管内皮細胞を分離・培養し，十分な細胞数まで増やした後に心臓弁scaffoldへ播種する方法を検討した。心臓弁は複雑な形状であるため細胞浮遊液中への単純な静置では表面全体に均一に播種できないことから，採血管用ローラー撹拌器を改良した2軸回転バイオリアクターと遠心型血液ポンプを利用した循環型バイオリアクターを独自に開発し，順に4時間および2日間の播種・培養を行うことで，心臓弁全体を内皮細胞でconfluentに覆うことに成功した。

この方法を用いて，Triton X-100により脱細胞化したブタ肺動脈弁に宿主内皮細胞を播種してから同所性に同種移植を行い，細胞播種を行わないで移植した脱細胞化弁，凍結保存弁と移植後成績を比較した。細胞播種脱細胞化弁では移植後1カ月の時点で内腔表面が一層の内皮細胞に覆われ，3カ月までに組織内部の再細胞化（平滑筋細胞，線維芽細胞）が進行した。一方，未播種の脱細胞化弁や凍結保存弁では内皮細胞による被覆までは同様に認められたが，その後の組織内再細胞化が進展せず，また凍結保存弁においては脱細胞化弁と比べて炎症細胞の浸潤が顕著であった[9]。従って，われわれの開発したバイオリアクターによる血管内皮細胞播種が移植弁組織の早期再細胞化に有用であると考えられた。現在，超高圧処理した脱細胞化弁とバイオリアクターによる内皮細胞播種を組み合わせた移植の検討を行っており，将来的には組織の再構築をさらに促進する目的で幹細胞を含めた複数の細胞種を導入したテーラーメード型移植用心臓弁の開発を計画している（図2）。

気管

悪性腫瘍や良性疾患による瘢痕・狭窄などにより気管のlong segmentを切除すると，再建に何らかの補填が必要となるため，人工気管や同種・異種気管の移植可能性が検討されてきた。そして，気管においても凍結保存や界面活性剤などによりドナー細胞（特に上皮細胞，軟骨細胞）を除去することで，移植時の抗原性が著しく減弱することが各種の動物実験において報告されている[6-8]。

われわれは，超高圧処理により脱細胞化したブタ気管をscaffoldとして移植利用する目的で，同法を他の脱細胞処理法（凍結保存およびTriton X-100処理）と比較検討した。超高圧処理気管は980 MPa（10,000気圧），

図2　再生型異種心臓弁移植シェーマ（文献5より引用）

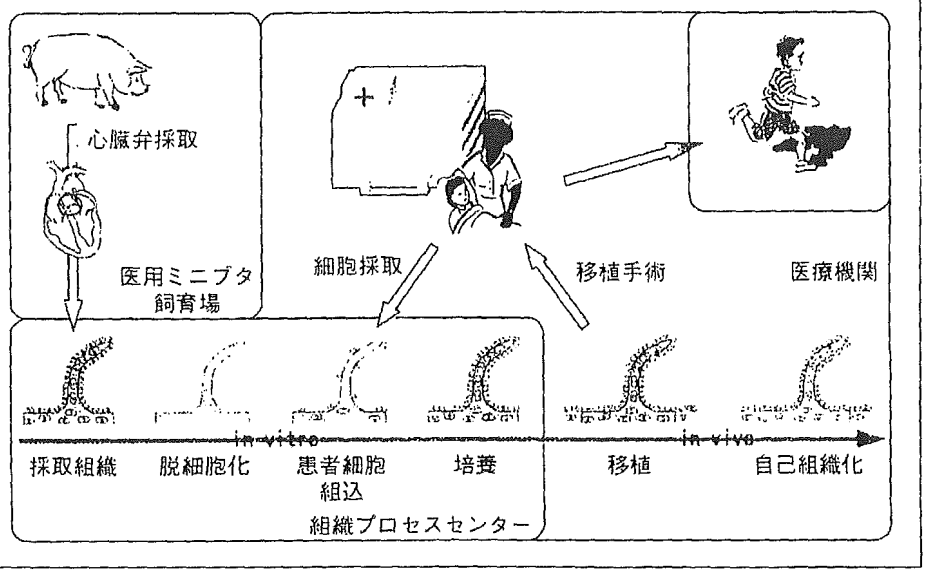

4℃で10分間加圧後，2週間緩徐に震盪洗浄し，その後PBS中に浸漬し4℃の冷所にて保存した。凍結保存気管は液体窒素にて急速冷却後，−80℃で凍結保存した。Triton X-100処理気管は1% Triton X-100溶液で24時間処理した後，2週間洗浄し，その後PBS中に浸漬し4℃の冷所にて保存した。各処理気管の病理像を比較すると，凍結保存では当然のことながら気管組織内に細胞成分がほぼ完全に残存しており，Triton X-100処理後も浅部組織の細胞成分は消失したものの軟骨内はほとんど除去できていなかった。一方，超高圧処理を行った気管では軟骨部細胞成分の残存が他の処理法に比べ少なかった（図3）[9]。今後，さらに軟骨部細胞成分の除去を徹底するため，超高圧処理の時間や回数，また超音波処理との組み合わせ等を検討する予定である。気管では移植後に管腔構造を保持する必要があるため，気管の圧縮試験を行い各処理気管で軟骨の力学強度を比較した。すると，Triton X-100処理気管は超高圧処理，凍結処理気管と比較して力学強度が約60%にまで低下していた。また，PERV-DNAは超高圧処理気管でのみ除去された。

次いで，ラットを用いた同種気管移植実験を行った。B-Nラットの気管を凍結保存，Triton X-100処理および超高圧処理したところ，Triton X-100処理気管では

図3　脱細胞化したブタ気管の組織像

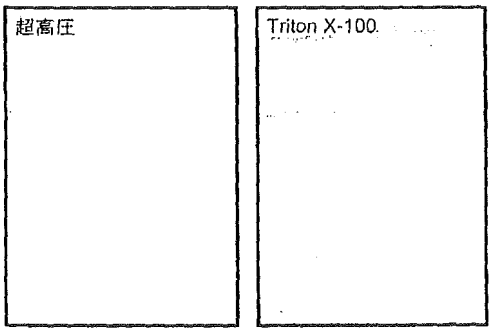

管腔構造が維持できないほどに軟骨強度が低下したため移植困難と判断し，凍結保存気管と超高圧処理気管をLewisラットへ同所性に移植した。4週間後に摘出し病理検査を行うと，両処理気管とも上皮の再生は比較的良好であったが，軟骨部にはほとんど新たな細胞は認められなかったため，軟骨部の再細胞化を早期に誘導する工夫が必要と考えられた。間葉系幹細胞は軟骨を含む各種細胞への分化が明らかとなっていることから[10]，現在われわれは，宿主の間葉系幹細胞を移植時に気管scaffoldに導入することで軟骨部も含めた早期再細胞化を実現するべく，その至適導入方法を検討

している。さらに，超高圧処理したブタ気管scaffoldについても，将来的な臨床応用を目指し同種・異種移植実験を計画している。

おわりに

われわれの開発した超高圧処理法による生体組織の脱細胞化について概説した。同種・異種組織scaffoldの作製法として本法は，組織深部まで脱細胞化を行うことができるとともに，組織の力学特性保持やウィルスを含む滅菌などの点で従来法と比較して優れていると考えられ，さらに保存時に凍結の必要がないため保存や輸送に関してもメリットがあると考える。われわれは，脱細胞化処理した組織scaffoldに宿主の自己細胞を組み合わせた再生型組織移植の臨床化の早期実現を目指し，研究を続けている。

文 献

1) 高圧生物科学と高圧技術. 鈴木敦士, 林 力丸編. 京都: さんえい出版, 1997.
2) Elkins RC, Goldstein S, Hewitt CW, *et al.* Recellularization of heart valve grafts by a process of adaptive remodeling. Semin Thorac Cardiovasc Surg 2001; 13: 87-92.
3) Teebken OE, Puschmann C, Aper T, *et al.* Tissue-engineered bioprosbtetic venous valve: a long-term study in sheep. Eur J Vasc Endovasc Surg 2003; 25: 305-312.
4) Korossis SA, Fisher J, Ingham E. Cardiac valve replacement: a bioengineering approach. Biomed Mater Eng 2000; 10: 83-124.
5) 藤里俊哉, 北村惣一郎. 生物組織スキャフォールドを用いたテーラーメード心臓弁. 循環器病研究の進歩 2003; 43: 65-71.
6) Yokomise H, Inui K, Wada H, *et al.* Long-term cryopreservation can prevent rejection of canine tracheal allografts with preservation of graft viability. J Thorac Cardiovasc Surg 1996; 111: 930-934.
7) Liu Y, Nakamura T, Yamamoto Y, *et al.* Immunosuppressant-free allotransplantation of the trachea: The antigenicity of tracheal grafts can be reduced by removing the epithelium and mixed glands from the graft by detergent treatment. J Thorac Cardiovasc Surg 2000; 120: 108-114.
8) Murakawa T, Nakajima J, Motomura N, *et al.* Successful allotransplantation of cryopreserved tracheal grafts with preservation of the pars membranacea in nonhuman primates. J Thorac Cardiovasc Surg 2002; 123: 153-160.
9) 角田卓也, 西岡宏, 舩本誠一, 他. 異種移植を目指した気管Scaffoldの開発－超高圧処理による脱細胞化－. 生体医工学 2004; 42: 36.
10) Wakitani S, Goto T, Pineda SJ, *et al.* Mesenchymal cell-based repair of large, full-thickness defects of articular cartilage. J Bone Joint Surg Am 1994; 76: 579-592.

Poly(lactide) Swelling and Melting Behavior in Supercritical Carbon Dioxide and Post-Venting Porous Material

Tomoko Fujiwara,[†,‡] Tetsuji Yamaoka,[§] Yoshiharu Kimura,[§] and Kenneth J. Wynne*[,†]

Chemical Engineering Department, School of Engineering, Virginia Commonwealth University, 601 West Main St., Richmond, Virginia 23284-3028, and Department of Polymer Science and Engineering, Kyoto Institute of Technology, Matsugasaki, Kyoto 606-8585, Japan

Received February 8, 2005
Revised Manuscript Received March 29, 2005

Introduction

Supercritical CO_2 has attracted considerable attention as an environmentally benign solvent for polymer synthesis, fractionation, swelling, and other processes. In addition, supercritical CO_2 can lower processing temperatures by reducing glass transition temperatures (T_g) or melting points (T_m).[1] The effects of temperature and pressure on processing behavior have been studied by a variety of methods.[2] We have developed a linear variable differential transformer (LVDT) technique to study polymer swelling by supercritical CO_2 under equilibrium conditions at high temperatures and pressures.[3] The LVDT method accurately captures increases in linear dimensions due to swelling and decreases at the onset of T_m (or T_g) in situ. We previously reported supercritical CO_2 plasticization and melting behavior for poly(vinylidene fluoride) (PVDF) using the LVDT method. PVDF showed swelling and melting behavior that was strongly dependent on temperature and pressure.[4]

Supercritical CO_2 has also been utilized extensively in basic studies, plasticization, and processing of biopolymers. The phase behavior of supercritical CO_2 solutions of poly(lactide) (PLA) as a function of pressure and temperature have been investigated.[5,6] Muller generated PLA microspheres by introducing a polymer solution into supercritical CO_2.[7] Rapid expansion of supercritical CO_2 solutions generated microspheres that were proposed as drug carriers.[8,9] Mooney and Langer have utilized CO_2 as a blowing agent to generate closed and open cell porosity.[10,11] Park utilized a combination of CO_2 foaming, salt leaching, and freeze-drying to obtain open cell structures.[12] Supercritical CO_2 foaming of PLA has been reported by Pishko et al.[13] and recently by others.[14]

While a key reason for using supercritical CO_2 is its environmentally benign nature, most of the processes described above have employed some combination of supercritical CO_2 with solvent casting, salt leaching, or water wash. Moreover, the precise swelling behavior of PLA in supercritical CO_2 is unclear. Here, we investigate swelling of D-lactide/L-lactide compositions in supercritical CO_2 using the LVDT method. Because pressure was released rapidly after LVDT measurements, porous structures resulted. Post-LVDT PLA was characterized DSC and SEM. The knowledge obtained in this research about the interaction between PLA and supercritical CO_2 may facilitate environmentally compatible polymer processing for biomaterials.

Experimental Section

Liquid CO_2 (99.8%) was obtained from Roberts Gas Company. PLA samples were received as injection molded plaques from Shimadzu Corporation (Kyoto). The molding conditions are as follows: melt temperature, 130−200 °C; injection pressure, 1177 bar; molding temperature, 40 °C; molding time, 25 s. Table 1 lists the as-received sample properties provided by Shimadzu. The optical purity (OP) of PLAs having different D-lactide/L-lactide compositions was evaluated using Shimadzu HPLC (chiral column) data according to eq 1:[15,16]

$$\%ee = ([L] - [D])/([L] + [D]) \times 100 \qquad (1)$$

The number in the sample designation indicates the percentage L-lactide present. PLA99.0, 96.1, and 95.8 are semicrystalline while PLA90.0 and 72.5 are amorphous. For swelling measurements in supercritical CO_2, rectangular bars (~9 × 3 × 2.5 mm) were cut from the molding plate with a small saw. The mass of a typical sample was about 0.1 g. The LVDT apparatus and procedures are described in detail previously.[3,4] In summary, the sample was placed on a small graphite stand and the follower rod was carefully mounted as shown in Figure 1. The follower rod has a cylindrical magnet screwed on top. Changes in sample dimensions cause the magnet to move in the coil generating a voltage that is converted to distance by prior calibration. Pressure and temperature are monitored and controlled as previously described.[3,4] Percent linear swelling is calculated as the change of length (ΔL) compared to initial length (L_0), i.e., linear swelling % = $(L_0 - L)/L_0 = \Delta L/L_0 \times 100$.

For semicrystalline PLAs, the sample chamber was heated to 50 °C, CO_2 was introduced, and the pressure was increased to 414 bar. Our equipment can operate at a maximum of about 680 bar. The 414 bar pressure was arbitrarily chosen for the survey reported herein. For amorphous PLAs, the pressure was raised to only 69 bar since softening occurs at low temperatures under CO_2 pressure. The pressure was kept constant during heating. Temperature was increased stepwise and dimensional changes were monitored at each interval until a constant value was obtained, typically 15 min. Finally, a decrease in linear swelling signaled the onset of melting or softening. At this point, CO_2 was vented and heating was terminated. The system cooled to ambient temperature within a few hours; sample recovery was usually accomplished the day after LVDT measurements.

* To whom correspondence should be addressed. E-mail: kjwynne@vcu.edu.
† Virginia Commonwealth University.
‡ Current address: Department of Chemistry, Boise State University, Boise, Idaho.
§ Kyoto Institute of Technology.

10.1021/bm050101v CCC: $30.25
Published on Web 05/03/2005

Table 1. PLA Compositions and Characterization Data

	properties[a]				CO_2 processing conditions and data		
		GPC			processing	softening	maximum
sample	HPLC OP (%ee)	M_w (×10⁴)	M_w/M_n	density (g/cm³)	P (bar)	T_m (°C)	$\Delta L/L$ (%)
PLA 99.0	98.0	20.2	2.5	1.2577	414	105	7.8
PLA 96.1	92.2	16.8	2.5	1.2601	414	92	9.1
PLA 95.8	91.6	15.5	2.4	1.2590	414	88	11.2
PLA 90.0	80.0	19.1	2.4	1.2614	69	–	0
PLA 72.5	45.0	15.3	2.8	1.2651	69	–	0

[a] Data from Shimadzu Corporation, Kyoto, Japan.

Table 2. DSC and MDSC Results

	as received						post-supercritical CO_2						
sample	T_g[a] (°C)	T_c[b] (°C)	T_m[b] (°C)	ΔH_c (J/g)	ΔH_f (J/g)	X_c (%)	T_g[a] (°C)	T_c[b] (°C)	T_m[b] (°C)	ΔH_c (J/g)	ΔH_f (J/g)	X_c (%)	% inc[d]
PLA 99.0	63.4	104.0	173.8	23.7	42.4	13.9	67.0	ND[c]	176.7	ND[c]	48.2	35.7	157
PLA 96.1	60.6	113.2	156.6	11.7	22.0	7.6	62.7	ND[c]	156.6	ND[c]	33.2	24.6	224
PLA 95.8	62.7	116.1	154.1	7.0	13.9	5.1	61.8	ND[c]	157.5	ND[c]	29.2	21.6	324
PLA 90.0	60.3	ND[c]	ND[c]				60.4	93.1	126.6	3.3	7.3	3.0	
PLA 72.5	52.5	ND[c]	ND[c]				54.2	ND[c]	ND[c]				

[a] By MDSC. [b] By DSC. [c] ND = not detected. [d] % increase in crystallinity = $(X_{c(\text{post-}CO_2)} - X_{c(\text{as-received})})/X_{c(\text{as-received})} \times 100$.

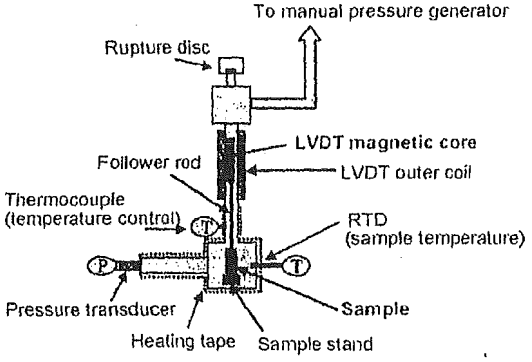

Figure 1. Schematic for the LVDT apparatus.

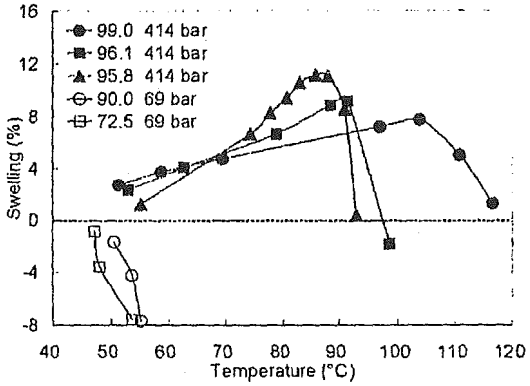

Figure 2. Linear percent swelling ($\Delta L/L_0 \times 100$) for PLAs in supercritical CO_2 as a function of temperature; (●) PLA99.0, (■) PLA96.1, and (▲) PLA95.8 at 414 bar; (○) PLA90.0 and (□) PLA72.5 at 69 bar.

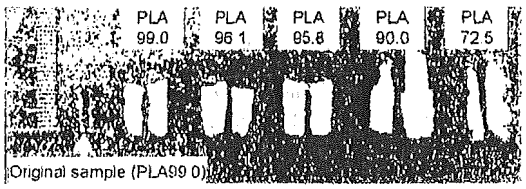

Figure 3. Photograph of as-received PLA99.0 and samples foamed by supercritical CO_2.

Thermal analysis measurements were carried out in a nitrogen atmosphere using TA-Q Series Q1000 DSC provided by TA Instruments. In a typical procedure, a 5 mg sample was heated at 10 °C/min from 0 to 200 °C. Modulated DSC (MDSC) was performed at a heating rate of 3 °C/min and modulation amplitude ±0.5 °C, 30 s. The data were analyzed by TA-Q Series software to separate total heat flow into the reversing and nonreversing components. PLA foams were fractured in liquid nitrogen and observed by scanning electron microscope (SEM) performed with a Hitachi SEM-S3000N.

Results and Discussion

PLA percent linear swelling as a function of temperature is shown in Figure 2. For semicrystalline PLAs at 414 bar, an increasing temperature resulted in a maximum swelling of 11.2% for PLA 95.8. From the swelling behavior (Figure 2), the order of CO_2 swelling at 414 bar is PLA99.0 < PLA96.1 < PLA95.8.

The swelling of semicrystalline polymers can be expressed as a sum of the mixing and elastic contributions based on the analogy of cross-linked network swelling.[4,17] Thus, the free energy change can be written according to eq 2

$$\Delta G_{swell} = \Delta G_{mixing} + \Delta G_{elastic} \quad (2)$$

The polymer−solvent (PLA−CO_2) interactions are included in the mixing contribution (ΔG_{mixing}). Swelling increases with the number and strength of the polymer−solvent interactions in comparison to polymer−polymer and solvent−solvent

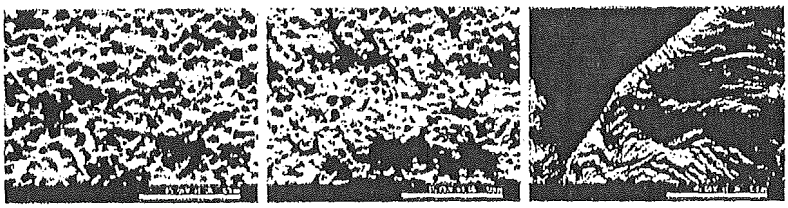

Figure 4. Typical scanning electron micrographs of supercritical CO_2 treated samples, PLA99.0, PLA95.8, and PLA72.5, fractured in liquid nitrogen. Scale bar is 50 μm.

interactions. The elastic contribution ($\Delta G_{elastic}$) incorporates the constraining effect of the crystalline junction points and resistance to swelling which is a function of polymer modulus. Increasing number of junction points (or cross-links) decreases swelling. This accounts for the observation that maximum swelling occurs for PLAs with low crystallinity, that is, minimum physical cross-links.

For semicrystalline PLAs, a turnover in the swelling–temperature curve occurs at T_m. The melting point is chosen as the mid-temperature of the first major decrease in linear dimension.[4] It is understood that not all polymer chains have melted at this temperature in the same way that not all polymer chains are melted at a peak in a DSC melting endotherm.[4] Melting of the entire crystalline phase occurs about 5–7 degrees higher. Melting temperatures and maximum values of $\Delta L/L_0$ are listed in Table 1. PLA melting points in supercritical CO_2 are remarkably lower (ΔT = 65–69 °C) than those obtained by DSC at ambient pressure (Table 2). Ambient temperature T_m's agree with previously reported values.[16]

The lowering of T_m is unexpectedly large for semicrystalline PLAs considering linear swelling is 11% or less. Our previous work showed that poly(vinylidene fluoride), PVDF, also displays modest swelling with a maximum of 12% at 130 °C and 670 bar.[4] However, the maximum T_m depression for PVDF is only 23 °C (135 °C at 483 bar).

PLA90.0 and PLA72.5 have T_g's at 60.4 and 54.2, respectively (Table 2). For these amorphous PLAs, softening occurred at the entry temperature of 50 °C after introduction of CO_2 (69 bar). Increasing temperature resulted in further decreases in linear dimensions characteristic of softening due to exceeding T_g. Thus, T_g for amorphous PLAs is lowered to 50° or less by relatively low CO_2 pressure.

At the highest temperature indicated for each sample (Figure 2), CO_2 was vented; that is, the system was pressure quenched. Figure 3 is a photograph of the resulting foamed PLAs. The original molded samples are transparent, whereas the foamed samples from pressure-quenching are white and their volume increased ≈500%. The volume of the sample chamber was insufficient for complete free expansion, so that there is potential for introducing larger pore volumes.

Figure 4 shows typical scanning electron micrographs of post-CO_2 PLA fractured in liquid nitrogen. Porous structures are observed for all semicrystalline PLAs, but not for amorphous PLAs. The average pore diameters calculated from SEM images are 5.4 ± 0.6 μm and 3.3 ± 0.5 μm for PLA99.0 and PLA95.8, respectively, suggesting a dependence on crystallinity. From the SEM images, pores in

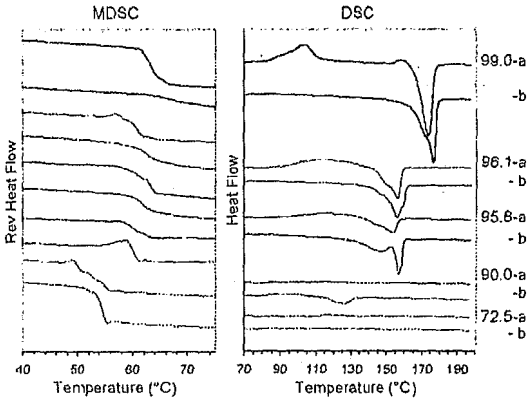

Figure 5. Left: Reversible heat flow curves of PLAs by MDSC (3 °C/min) and modulation amplitude ±0.5 °C, 30 s. Right: DSC heat flow curves for PLAs (10 °C/min); (a) as-received PLAs and (b) PLAs foamed by supercritical CO_2.

semicrystalline PLAs appear to be closed cell. Smaller pore size (PLA95.8) correlates with lower crystallinity under these processing conditions. Under the limited conditions investigated open cell structures, which are required for tissue engineering, were not obtained.

Representative DSC and MDSC curves of as-received and supercritical CO_2 foamed PLA are shown in Figure 5, and the results are summarized in Table 2. As received PLA99.0 shows a distinct T_g at 63.4 °C in the reversing heat flow curve by MDSC and crystallization and melting at 173.8 °C by conventional DSC. Post-CO_2 PLAs generally have somewhat higher T_g's and T_m's. The crystallinity of as-received and post-CO_2 PLA is estimated from the enthalpy of fusion (ΔH_f) and crystallization (ΔH_c) according to eq 3

$$\%X_c = \frac{\Delta H_f - \Delta H_c}{\Delta H_f^\circ} \times 100 \qquad (3)$$

The value of the ΔH_f° for perfectly crystalline PLA has been reported from 83 to148 J/g.[18] It is difficult to estimate ΔH_f° because of dependence on processing history. If we chose the recent value of Miyata and Masuko for ΔH_f° (135 J/g),[19] the degree of crystallinity for as-received PLA99.0 is 13.9%. Crystallinity increases to 35.7% for post-CO_2 PLA99.0, an increase of 157%. Crystallinity also increased for PLA96.1 (224%) and PLA95.8 (324%). Crystallinity of PLA90.0 could not be detected by DSC but post-CO_2 PLA90.0 had a crystallinity of 3.0%.

Conclusion

We have observed a remarkable lowering of T_m for semicrystalline PLA and a lowering of T_g for amorphous PLA in supercritical CO_2. Percent linear swelling by supercritical CO_2 increased with decreasing crystallinity. Porous post-supercritical CO_2 PLAs have higher crystallinities than as received plaques. Our results suggest that generating porous PLA by supercritical CO_2 assisted processing using different temperatures, pressures, and initial PLA crystallinity may control the pore size and porosity.

For specialty biomedical applications, supercritical CO_2 assisted processing may have advantages that overcome the expense of using high-pressure equipment. These advantages include volatile-organic-solvent (VOC) free processing, water free processing that can prevent PLA hydrolysis, and potentially lowered processing temperatures. The latter two advantages may maintain high molecular weight, which in turn provides improved mechanical properties. Increased crystallinity may change the rate of hydrolysis and therefore rates of drug delivery.

Acknowledgment. We gratefully acknowledge funding for high-pressure equipment from Daikin Institute of Advanced Chemistry and Technology (DAI-ACT). We acknowledge the help of Dr. Suresh Shenoy in making LVDT measurements.

References and Notes

(1) Wissinger, R. G.; Paulaitis, M. E. *J. Polym. Sci., Part B: Polym. Phys.* **1991**, *29*, 631.
(2) (a) McHugh, M. A.; Krukonis, V. J. *Supercritical Fluid Extraction*; Butterworth-Heimann: London, 1994. (b) Cooper, A. I. *J. Mater. Chem.* **2000**, *10*, 207.
(3) Shenoy, S. L.; Weerdeman, D.; Sebra, R.; Garach-Domech, A.; Wynne, K. J. *Macromol. Rapid Commun.* **2002**, *23*, 1130−1133.
(4) Shenoy, S. L.; Fujiwara, T.; Wynne, K. J. *Macromolecules* **2003**, *36*, 3380−3385.
(5) Lee, J. M.; Lee, B. C.; Hwang, S. J. *J. Chem. Eng. Data* **2000**, *45*, 1162−1166.
(6) Conway, S. E.; Byun, H. S.; McHugh, M. A.; Wang, J. D.; Mandel, F. S. *J. Appl. Polym. Sci.* **2001**, *80*, 1155−1161.
(7) Bleich, J.; Muller, B. W.; Wassmus, W. *Int. J. Pharm.* **1993**, *97*, 111−117.
(8) Tom, J. W.; Lim, G. B.; Debenedetti, P. G.; Prudhomme, R. K. *ACS Symp. Ser.* **1993**, *514*, 238−257.
(9) (a) Kim, J. H.; Paxton, T. E.; Tomasko, D. L. *Biotechnol. Progr.* **1996**, *12*, 650−661. (b) Falk, R. F.; Randolph, T. W. *Pharm. Res.* **1998**, *15*, 1233−1237. (c) Elvassore, N.; Bertucco, A.; Caliceti, P. *J. Pharm. Sci.* **2001**, *90*, 1628−1636. (d) Taki, S.; Badens, E.; Charbit, G. *J. Supercrit. Fluids* **2001**, *21*, 61−70. (e) Ghaderi, R.; Artursson, P.; Carlfors, J. *Eur. J. Pharm. Sci.* **2000**, *10*, 1−9. (f) Breitenbach, A.; Mohr, D.; Kissel, T. *J. Controlled Release* **2000**, *63*, 53−68.
(10) Mooney, D. J.; Baldwin, D. F.; Suh, N. P.; Vacanti, L. P.; Langer, R. *Biomaterials* **1996**, *17*, 1417−1422.
(11) Harris, L. D.; Kim, B. S.; Mooney, D. J. *J. Biomed. Mater. Res.* **1998**, *42*, 396−402.
(12) Nam, Y. S.; Yoon, J. J.; Park, T. G. *J. Biomed. Mater. Res.* **2000**, *53*, 1−7.
(13) Hile, D. D.; Amirpour, M. L.; Akgerman, A.; Pishko, M. V. *J. Controlled Release* **2000**, *66*, 177−185.
(14) (a) Singh, L.; Kumar, V.; Ratner, B. D. *Biomaterials* **2004**, *25*, 2611−2617 (b) Fujimoto, Y.; Ray, S. S.; Okamoto, M.; Ogami, A.; Yamada, K.; Ueda, K. *Macromol. Rapid Commun.* **2003**, *24*, 457−461.
(15) Urayama, H.; kanamori, T.; Kimura, Y. *Macromol. Mater. Eng.* **2001**, *286*, 705.
(16) Urayama, H.; Moon, S.-I.; Kimura, Y. *Macromol. Mater. Eng.* **2003**, *288*, 137−143.
(17) Flory, P. J. *Principles of polymer chemistry*; Cornell University Press: Ithaca, NY, 1953.
(18) (a) Fischer, E. W.; Sterzel, F.; Wegner, H. J. *Kolloid-Z. Z. Polym.* **1973**, *251*, 980. (b) Cohn, D.; Younes, H.; Marom, G. *Polymer* **1987**, *28*, 2018. (c) Kalb, B.; Pennings, A. J. *Polymer* **1980**, *21*, 607. (d) Gilding, D. K.; Reed, A. M. *Polymer* **1979**, *20*, 1459. (e) Sarasua, J. R.; Prud'homme, R. E.; Wisniewski, M.; Le Borgne, A.; Spassky, N. *Macromolecules* **1998**, *31*, 1, 3895−3905. (f) Huang, J.; Lisowski, M. S.; Runt, J.; Hall, E. S.; Kean, R. T.; Buehler, N.; Lin, J. S. *Macromolecules* **1998**, *31*, 2593−2599.
(19) Miyata, T.; Masuko, T. *Polymer* **1998**, *39*, 5515−5521.

BM050101V

Available online at www.sciencedirect.com
SCIENCE DIRECT®
Analytical Biochemistry 340 (2005) 369–372
ANALYTICAL BIOCHEMISTRY
www.elsevier.com/locate/yabio

Notes & Tips

Analytical method for estimation of kinetics of oligonucleotide/RNA hybridization using fluorescence depolarization spectroscopy

Takashi Sakamoto [a], Atsushi Mahara [a], Reiko Iwase [b], Tetsuji Yamaoka [a], Akira Murakami [a,*]

[a] *Department of Polymer Science and Engineering, Kyoto Institute of Technology, Matsugasaki, Sakyo-ku, Kyoto 606-8585, Japan*
[b] *Department of Bioscience, Teikyo University of Science and Technology, Yatsuzawa 2525, Uenohara, Kitatome-gun, Yamanashi 409-0193, Japan*

Received 20 August 2004
Available online 10 December 2004

Antisense-based technology, which makes it possible to specifically regulate the gene expression, has been expected to be a powerful tool for the chemotherapy of various diseases and for the investigation of gene functions. This technology is now in the clinical stage for the treatment of several cancers. However, the antisense method has not been well established as a general tool for this purpose, and some crucial problems remain to be solved. Especially, it is quite difficult to select the target site of an antisense oligonucleotide (ASON)[1] on the target mRNA, and this difficulty lies in the complexity of the tertiary structure of the target mRNA. The solution of the problem could contribute to the further development of the antisense method. Many researchers have worked to solve the problem by determination of the structural feature of the folded target RNA [1,2]. Recently, it was reported that the ASONs that can bind to the target mRNA with a higher association rate constant (k_{assoc}) represent the higher antisense effect [3,4]. Namely, the kinetics of the ASON/mRNA hybridization could be one of the key factors in designing effective ASONs. However, the throughputs of the methods, such as gel-electrophoresis [4], surface plasmon resonance analysis [5], and quartz crystal microbalance [6], which are frequently used for the estimation of the hybridization kinetics, are not high. Furthermore, the results which are obtained from those methods do not always reflect the real feature of the interaction in homogeneous solution. A more sophisticated analytical method, which can evaluate the kinetics under physiological conditions, is required.

This report focuses on this aspect, and we adopted a fluorescence-anisotropy-based analytical method for the purpose. Previously, we reported that this method can detect the hybridization between 5'-fluorescein-labeled oligodeoxyribonucleotide (F-probe) and *Escherichia coli* 5S rRNA under physiological conditions [7]. The fluorescence anisotropy of F-probe largely increased upon hybridization with 5S rRNA. In the report, we discussed the static interaction between F-probe and 5S rRNA. In contrast, as RNAs are dynamic in solution, information on the dynamic features of the hybridization is necessary to design ASONs. Therefore, in the present study, we tried to establish an analytical method for determination of an effective target site of ASONs based on the kinetics of the ASON/target mRNA hybridization. To evaluate this method, a certain mRNA should be used as the target molecule. However, as no information concerning the three-dimensional structure of mRNA has been reported, there is difficulty in demonstrating the appropriateness of the method described in this report. Therefore, as a model folded RNA, we chose *E. coli* 16S ribosomal RNA (16S rRNA), whose secondary structure has been already determined [8]. Recently, the tertiary structure was reported as a part of the 30S ribosomal subunit [9].

Based on the reported secondary structure of 16S rRNA [8], we selected seven single-strand regions (L1–

* Corresponding author. Fax: +81 75 724 7814.
E-mail address: akiram@kit.ac.jp (A. Murakami).

[1] *Abbreviations used:* ASON, antisense oligonucleotide; k_{assoc}, association rate constant; F-probe, 5'-fluorescein-labeled oligodeoxyribonucleotide; 16S rRNA, *Escherichia coli* 16S ribosomal RNA; cORN, complementary oligo-RNA; K_d, equilibrium dissociation constant; RNase H, human ribonuclease H; k_{dissoc}, dissociation rate constant.

doi:10.1016/j.ab.2004.11.037

L7) and one double-strand region (S1) as target sites of the F-probe (Fig. 1). The binding ability of the F-probe to 16S rRNA was examined by the fluorescence anisotropy analysis (Table 1). The addition of the complementary oligo-RNA (cORN, 15mer) to the F-probes caused a change in fluorescence anisotropy for all the F-probes, though the degrees of the increment varied. The addition of 16S rRNA to F-L1, F-L2, and F-L7 caused a significant change in fluorescence anisotropy, suggesting that F-L1, F-L2, and F-L7 bound to 16S rRNA. The addition of 16S rRNA to the rest of the F-probes did not appreciably affect the fluorescence anisotropy. Furthermore, significant change in fluorescence lifetime was not observed (Table 1). That is, it was concluded that the F-probes, whose fluorescence anisotropy did not changed by addition of 16S rRNA, did not bind to 16S rRNA. It was also suggested that the loop regions were not always an acceptable site for the ASONs.

To quantitatively evaluate the binding affinity of the F-probes to their target sites, the equilibrium dissociation constant (K_d) of the F-probe/16S rRNA hybrid was obtained from the titration analysis by the curve-fitting protocol according to the general equilibrium state binding theory (Table 1). Every K_d was greater than the typical K_d of the DNA/RNA hybrid (1–100 nM, 10 nt in length), indicating that the local secondary or tertiary structure of 16S rRNA might significantly affect the F-probe/16S rRNA hybrid formation. These results suggested that the stability of the F-L1/16S rRNA hybrid was similar to that of the F-L2/16S rRNA hybrid and that the stability of the F-L7/16S rRNA hybrid was lower than that of the F-L1 (F-L2)/16S rRNA hybrid. From the viewpoint of the K_d, it is concluded that L1 and/or L2 could be favorable sites in 16S rRNA for an ASON. Previously, we reported a similar investigation using the pyrene-modified 2'-OMe type oligo-RNA and 16S rRNA [10]. The

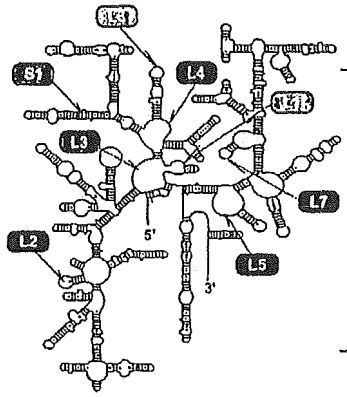

	Sequence (5' to 3')	Target site
F-L1	GCC GTA CTC C	L1 (887–896nt)
F-L2	CCG TGT CTC A	L2 (323–332nt)
F-L3	CAG TAA TTC C	L3 (557–566nt)
F-L4	ATC GTT TAC G	L4 (811–820nt)
F-L5	GAA CGT ATT C	L5 (1373–1382nt)
F-L6	GTA TCT AAT C	L6 (786–795nt)
F-L7	GCG TTG CAT C	L7 (963–972nt)
F-S1	GTA TCA GAT G	S1 (634–643nt)

Fig. 1. Target sites of F-probes on 16S rRNA and the oligonucleotide sequences of F-probes.

Table 1
Fluorescence anisotropy and mean lifetime of F-probes (r_p, τ_p) in the presence of cORN (r_{cORN}) or 16S rRNA (r_{rRNA}, τ_{rRNA}) 24 h after the addition of RNA to the F-probe and K_d, k_{assoc}, and k_{dissoc} of F-probes/16S rRNA hybrid formation

	r_p[a]	r_{cORN}[a]	r_{rRNA}[a]	τ_p (ns)[b]	τ_{rRNA} (ns)[b]	K_d (nM)[c]	k_{assoc} ($M^{-1}s^{-1}$)[d]	k_{dissoc} (s^{-1})[d]	Acceptability to 16S rRNA[e]
F-L1	0.041	0.045	0.080	0.9	2.5	180	$0.3 \times 10^3 (\pm 0.03 \times 10^3)$	$0.5 \times 10^{-4} (\pm 0.06 \times 10^{-4})$	Middle
F-L2	0.059	0.095	0.100	3.9	3.9	260	$6.1 \times 10^3 (\pm 0.40 \times 10^3)$	$15.7 \times 10^{-4} (\pm 0.90 \times 10^{-4})$	High
F-L3	0.055	0.077	0.051	3.5	3.7	n.d.[f]	n.d.	n.d.	Middle
F-L4	0.071	0.073	0.072	4.1	4.1	—	n.d.	n.d.	—
F-L5	0.074	0.080	0.077	2.3	2.1	—	n.d.	n.d.	—
F-L6	0.056	0.066	0.060	3.4	3.3	—	n.d.	n.d.	—
F-L7	0.069	0.090	0.075	3.4	3.3	960	$1.2 \times 10^3 (\pm 0.07 \times 10^3)$	$11.4 \times 10^{-4} (\pm 0.70 \times 10^{-4})$	—
F-S1	0.048	0.057	0.048	2.2	2.5	n.d.	n.d.	n.d.	Not acceptable

[a] [F-probe] = [16S rRNA] (or [cORN]) = 0.75 μM in 10 mM Tris–HCl (pH 7.5), 100 mM NaCl, and 1 mM $MgCl_2$. The excitation wavelength was 495 nm with observation at 515 nm and a band-pass of 5 nm at 11 °C.
[b] τ was estimated by exponential fitting with nonlinear least square method from fluorescence decay curve.
[c] K_d values were calculated by the curve-fitting protocol of the titration curves of the F-probe and 16S rRNA.
[d] Kinetic parameters were calculated by curve-fitting of the time course of the fluorescence anisotropy change (Fig. 2).
[e] Acceptability was estimated from the increment in equilibrium-state fluorescence intensity of equimolar mixture of pyrene-modified 2'-OMe type oligo-RNA and 16S rRNA [10].
[f] Not detected.

method was based on the drastic change in the fluorescence intensity of the pyrene upon hybridization. Regions L1 and L2 were found to be the acceptable sites while S1 was not. The results agreed well with the present study except for the case of L3. This exception could be due to the structural characteristics of the fluorescent oligonucleotide used.

The static information of the hybridization, i.e., K_d, has been frequently used for the determination of optimal antisense sequence, and ASONs, whose sequences are determined with only the static information, are not always effective. We tried to solve this problem from the viewpoint of kinetics. The target RNAs transcribed in the nucleus are promptly modulated by various proteins competing with ASON. It was assumed that ASONs, which take a long time to hybridize with mRNA, might not be effective. Recently, some researchers reported the importance of the kinetic aspect to the antisense efficacy. Walton et al. [3] investigated the correlation between the hybridization kinetics and the human ribonuclease H (RNase H) activity, which is one of the major mechanisms of the antisense effect. They concluded that the k_{assoc} could be a useful indicator for selecting effective antisense sequences. Haruki et al. [11] reported that the k_{assoc} of the interaction between *E. coli* ribonuclease HI and DNA/RNA hetero-duplex was about $10^6\,M^{-1}s^{-1}$. As the k_{assoc} of the hybridization of oligonucleotide and the folded RNA was about 10^3–$10^5\,M^{-1}s^{-1}$ [3,4], it was found that the binding of oligonucleotides to the target RNA was the rate-determining step of the cleavage reaction of the target RNA by RNase H. These reports suggest the importance of the kinetic analysis of the interaction between the ASON and its target mRNA, and for this purpose a method that can evaluate the kinetics in homogeneous physiological media or in cells is required. In the present study, to obtain the kinetic information on the interaction between the F-probe and the 16S rRNA, the time course of the change in fluorescence anisotropy was measured in homogeneous physiological solution (Fig. 2). Significant time-dependent change in fluorescence anisotropy was observed in L1 (Fig. 2A, ○), L2 (Fig. 2A, ●), and L7 (Fig. 2B, ▽). These results indicated that the time to attain the equilibrium state was varied with the sites in 16S rRNA. The k_{assoc} and dissociation rate constant (k_{dissoc}) were obtained by the curve-fitting protocol according to the general binding kinetics theory (Table 1). The parameters for F-L3, F-L4, F-L5, F-L6, and F-S1 could not be obtained because of the poor binding ability to 16S rRNA. The k_{assoc} for L1, L2, and L7 were in the range of $10^3\,M^{-1}s^{-1}$, which were in good accordance with the results of Walton et al. [3] and Venturini et al. [4]. These results suggested that this method could be applicable for the kinetic-based selection of antisense sequences in homogeneous physiological solution. In the present study, it is concluded that L2, which shows the largest

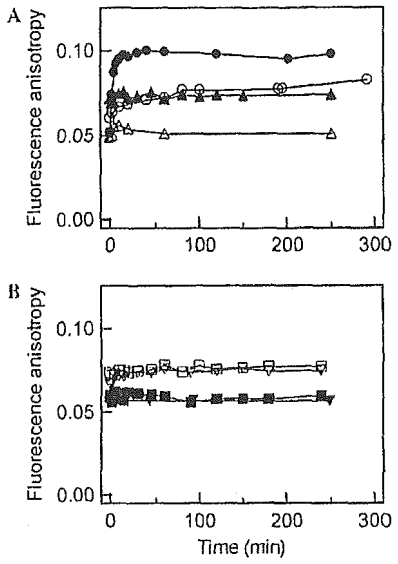

Fig. 2. Time courses of the fluorescence anisotropy change in the F-probes caused by the addition of 16S rRNA. (A) Profiles of (○) F-L1, (●) F-L2, (△) F-L3, and (▲) F-L4. (B) Profiles of (□) F-L5, (■) F-L6, (▽) F-L7, and (▼) F-S1. [F-probe] = [16S rRNA] = 0.6 μM in the same buffer system and condition as in Table 1.

k_{assoc} among the sites chosen, was the most favorable target site of the ASON and that L1, which has K_d similar to that of L2, was the second candidate region of the ASON.

As our method dose not require the bound/free separation protocol, the kinetic parameters of the hybridization can be easily obtained by simple mixing of the F-probe and RNA. This convenient protocol might largely contribute to the high-throughput screening of the effective antisense sequence.

In conclusion, it was demonstrated that both K_d and kinetic parameters (k_{assoc} and k_{dissoc}) of the oligonucleotide/RNA hybrid formation could be used for the design of ASON along with fluorescence anisotropy analysis. Therefore, this analytical method might play a significant role in the screening of efficient ASONs with kinetic aspects. Further development of this method using mRNA, whose tertiary structure is unknown, is now underway in conjunction with the in vitro translation study.

Acknowledgments

This research was partly supported by a Grant-in-aid for Scientific Research (No. 14580609, A.M., T.Y., R.I.) and by Grants for Regional Science and Technology Promotion (A.M.) from the Ministry of Education, Science, Sports and Culture of Japan.

References

[1] B.H. Lloyd, R.V. Giles, D.G. Spiller, J. Grzybowski, D.M. Tidd, D.R. Sibson, Determination of optimal sites of antisense oligonucleotide cleavage within TNFalpha mRNA, Nucleic Acids Res. 29 (2001) 3664–3673.

[2] M. Zuker, A.B. Jacobson, Well-determined regions in RNA secondary structure prediction: analysis of small subunit ribosomal RNA, Nucleic Acids Res. 23 (1995) 2791–2798.

[3] S.P. Walton, G.N. Stephanopoulos, M.L. Yarmush, C.M. Roth, Thermodynamic and kinetic characterization of antisense oligodeoxynucleotide binding to a structured mRNA, Biophys. J. 82 (2002) 366–377.

[4] F. Venturini, J. Braspenning, M. Homann, L. Gissmann, G. Sczakiel, Kinetic selection of HPV 16 E6/E7-directed antisense nucleic acids: anti-proliferative effects on HPV 16-transformed cells, Nucleic Acids Res. 27 (1999) 1585–1592.

[5] A.J. Thiel, A.G. Frutos, C.E. Jordan, R.M. Corn, L.M. Smith, In situ surface plasmon resonance imaging detection of DNA hybridization to oligonucleotide array on gold surfaces, Anal. Chem. 69 (1997) 4948–4956.

[6] Y. Okahata, Y. Matsunobu, K. Ijiro, M. Mukae, A. Murakami, K. Makino, Hybridization of nucleic acids immobilized on a quartz crystal microbalance, J. Am. Chem. Soc. 114 (1992) 8200–8299.

[7] A. Murakami, M. Nakaura, Y. Nakatsuji, S. Nagahara, Q. Tran-Cong, K. Makino, Fluorescent-labeled oligonucleotide probes: detection of hybrid formation in solution by fluorescence polarization spectroscopy, Nucleic Acids Res. 19 (1991) 4097–4102.

[8] R.R. Gutell, N. Larsen, C.R. Woese, Lessons from an evolving rRNA: 16S and 23S rRNA structures from a comparative perspective, Microbiol. Rev. 58 (1994) 10–26.

[9] B.T. Wimberly, D.E. Brodersen, W.M. Clemons Jr., R.J. Morgan-Warren, A.P. Carter, C. Vonrhein, T. Hartsch, V. Ramakrishnan, Structure of the 30S ribosomal subunit, Nature 407 (2000) 327–339.

[10] A. Mahara, R. Iwase, T. Sakamoto, T. Yamaoka, K. Yamana, A. Murakami, Detection of acceptor sites for antisense oligonucleotides on native folded RNA by fluorescence spectroscopy, Bioorg. Med. Chem. 11 (2003) 2783–2790.

[11] M. Haruki, E. Noguchi, S. Kanaya, R.J. Crouch, Kinetic and stoichiometric analysis for the binding of *Escherichia coli* ribonuclease H1 to RNA–DNA hybrids using surface plasmon resonance, J. Biol. Chem. 272 (1997) 22015–22022.

Facilitated Disassembly of Polyplexes Composed of Self-assembling Amphiphilic Polycations Enhances the Gene Transfer Efficacy

Tatsuya Kitagawa, Reiko Iwase, Kazuhiko Ishihara,† Tetsuji Yamaoka,*# and Akira Murakami
Department of Polymer Science and Engineering, Kyoto Institute of Technology, Matsugasaki, Sakyo-ku, Kyoto 606-8585
†*Department of Materials Engineering, School of Engineering, The University of Tokyo, 7-3-1 Hongo, Bunkyo-ku, Tokyo 113-8656*

(Received August 10, 2005; CL-051041)

Amphiphilic polycations, p(DMAPAA-*co*-MPC-*co*-SA)s, with various cation contents were designed as novel micelle-like nonviral gene carriers. The carriers led to a higher transgene expression in COS-1 cells three times as high as the case of the linear-type polycations. The enhanced transgene expressions were found to be related to the disassembly of plasmid DNA/carrier polyplexes. It can be concluded that a topological factor of the carriers greatly influences on the gene expression efficiency.

A variety of polycations with different chemical structures have been found to be effective gene carriers but still have lower efficiency than the viral vectors.[1-3] To improve it, each step in the gene transfer such as cellular uptake of polyplexes,[4] their release from the endosome,[5] and the localization into the nucleus[6] have been studied. In contrast, the transcription of the polyplexes, which is the last step of the gene transfer, was not well understood. We previously reported the enhanced gene expression by introducing nonionic hydrophilic groups to conventional poly(L-lysine) carrier.[7] This chemical modification was found to effectively suppress the polyplex compaction, and hence its transcription efficiency in the nuclei was greatly improved. In the present study, we have tried to improve the intranucleus transcription efficiency by changing the molecular topology of the polycation carriers from linear-type to micelle-like for the first time. Our working hypothesis was that the micelle-like polycations interact with DNA molecule with less entanglement than the linear-type ones. In order to prepare both liner-type and micelle-like carriers which have similar properties other than the topology, slight amount of hydrophobic moieties was introduced to the conventional linear polycations. The hydrophobized polycations are known to form a kind of micelle based on the self-aggregation mechanism.[8] A series of amphiphilic polycations containing 2-methacryloyloxyethylphosphoryl choline (MPC) were synthesized, and the micelle forming property and the gene transfection ability were investigated. Although MPC has been reported to act as a component of block polymer-type carriers, we selected this monomer as a nonionic hydrophilic monomer as previously reported.[9,10]

Random copolymerization of *N*-[3-(dimethylamino)propyl] acrylamide (DMAPAA), MPC, and stearyl acrylate (SA) were carried out in methanol using AIBN as an initiator (M/I = 200) at 60 °C for 4 h, dialyzed against methanol, and lyophilized (Figure 1). The compositions were determined by ^{1}H NMR. The copolymers were expressed as p(DMAPAA*x*-*co*-MPC*y*-*co*-SA*z*), where *x*, *y*, and *z* represent the molar composition of each monomers. DMAPAA content of the copolymers was similar to the monomer ratio in feed. The molecular weight determined by gel permeation chromatography (GPC) of

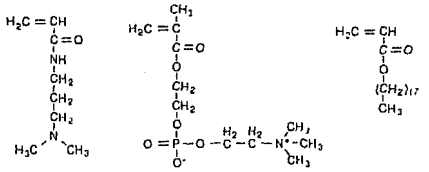

Figure 1. Chemical structures of used monomers.

p(DMAPAA46-*co*-MPC53-*co*-SA1), p(DMAPAA62-*co*-MPC37-*co*-SA1), p(DMAPAA40-*co*-MPC60), and p(DMAPAA62-*co*-MPC38) were, 52,000, 42,000, 102,000, and 65,000, respectively.

The critical micelle concentration (cmc) of the obtained polymers were measured using pyrene as hydrophobic probe molecules at various polymer concentrations from 0.01 to 1.0 g L^{-1}.[11] The fluorescent sensitization with an increased concentration was observed only for p(DMAPAA-*co*-MPC-*co*-SA)s, and red shift from 334 to 343 nm was observed, indicating that the amphiphilic polycations formed micelle-like structures in water. The cmc of p(DMAPAA46-*co*-MPC53-*co*-SA1) and p(DMAPAA62-*co*-MPC37-*co*-SA1) was 3.1 and 6.6 mg L^{-1}, respectively. Their particle sizes determined by DLS of 100 μg L^{-1} in filtered-Dulbecco's Modified Eagle's Medium were 280 ± 28 and 290 ± 34 nm, respectively.

pCMV-Luc endcoding luciferase gene and the copolymers were incubated in TE buffer for 30 min at room temperature resulting in the polyplex formation. The charge ratio of mixed plasmid DNA and polymers (C/A ratio) was ranged from 0.5 to 10.0. The agarose gel electrophoresis showed that the DNA formed polyplex at the C/A ratio higher than 1.0 completely. COS-1 cells were transfected with the polyplexes by the chloroquine method.[12]

The dependence of the transient expression on the C/A ratio was shown in Figure 2. Each polymer showed no cytotoxicity. As we previously proposed, the transgene expression was greatly affected by the polymer compositions due to the balance of the cationicity and nonionic hydrophilicity.[13] In the present study, the carriers having about 40% of cation contents showed higher gene expression, irrespective of the SA contents. When copolymers with similar DMAPAA contents were compared, p(DMAPAA-*co*-MPC-*co*-SA)s showed about three times higher expression than the p(DMAPAA-*co*-MPC)s. On the other hand, cellular uptake of polyplexes was not affected by the SA unit at all, and the amount of ^{32}P-labeled pDNA delivered using p(DMAPAA46-*co*-MPC53-*co*-SA1) and p(DMAPAA40-*co*-MPC60) was 13.2 ± 1.9 and 16.3 ± 0.6 ng/1.0 × 10^4 COS-1 cells, respectively. In addition, there was no big difference in the intracellular distribution when compared under a fluorescent micro-

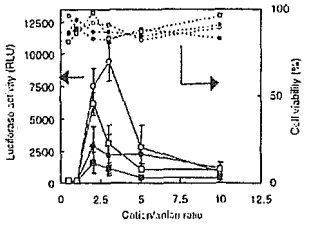

Figure 2. Expression of luciferase gene introduced to COS-1 cells using p(DMAPAA46-*co*-MPC53-*co*-SA1) (○), p(DMAPAA62-*co*-MPC37-*co*-SA1) (□), p(DMAPAA40-*co*-MPC60) (●), and p(DMAPAA62-*co*-MPC38) (■) and the cell viability.

scope (date not shown).

These results indicate that the higher efficiency of p(DMAPAA46-*co*-MPC53-*co*-SA1) was resulted from the efficient transcription of the transgene complexing with the micelle-like carriers after their internalization. We then examined the dissociation tendency of the polyplexes. The exchange reaction of DNA with anionic macromolecules, such as mRNA, sulfated sugars, and nuclear chromatin existing as essential cellular components was reported to occur during the intracellular trafficking.[12] A given amount of potassium polyvinyl sulfate (PVSK) was added to the polyplex (C/A ratio = 3). The unit mole ratio of PVSK and cationic copolymer was set to 0.8:1. The reaction mixture was incubated for 30 min at room temperature and evaluated on 0.8% agarose gel (Figure 3). PVSK did not affect on the mobility of free DNA. The clear difference in the easiness of polyplex dissociation was observed. Complete release of DNA from the polyplexes with p(DMAPAA46-*co*-MPC53-*co*-SA1) was observed by adding PVSK solution. In comparison, dissociation of the p(DMAPAA40-*co*-MPC60)/pDNA polyplexes has not occurred at all. The micelle-like structure is considered to facilitate the release of plasmid DNA from the polyplexes even in the intracellular environment.

In vitro transcription/translation experiment using TNT® T7 coupled Reticulocyte Lysate System (Promega Corporation, USA) was carried out for the p(DMAPAA46-*co*-MPC53-*co*-SA1)/pDNA polyplex suspentions in the presence or absence of PVSK. Briefly, reaction lysate (25 μL TNT® Rabbit Reticulocyte Lysate, 0.5 μL Amino Acid Mixture (1 mM), 2 μL TNT® Reaction Buffer, 1 μL TNT® T7 RNA Polymerase, 2 μL Rnase inhibitor (27.2 u/μL)) was added to pT7-Luc/carrier polyplex suspension (C/A ratio = 3) and incubated for 90 min at 37 °C, and the luciferase activity was measured. The luciferase activities for p(DMAPAA46-*co*-MPC53-*co*-SA1) /pDNA polyplex and free DNA were 1.0×10^5 and 5.1×10^5 RLU, respectively. The p(DMAPAA46-*co*-MPC53-*co*-SA1) suppressed the direct transcription of the plasmid DNA. On the other hand, when

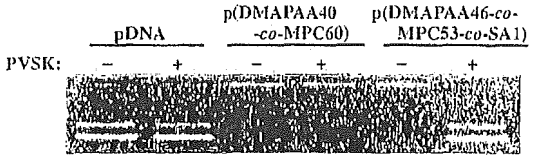

Figure 3. Disassembly of p(DMAPAA40-*co*-MPC60)/pDNA and p(DMAPAA46-*co*-MPC53-*co*-SA1)/pDNA polyplexes in the presence or absence of 0.8 mol % PVSK relative to the DMAPAA unit moles.

0.8 mol % of PVSK was added to this system, the activity was greatly recovered and reached 4.4×10^5 RLU, which is about 85% of the result for the free DNA. In contrast, p(DMAPAA40-*co*-MPC60)/pDNA shows 1.5×10^5 and 0.7×10^5 RLU in the presence or absence of PVSK, respectively. These results indicate that suppressed transcription can be recovered only for p(DMAPAA46-*co*-MPC53-*co*-SA1), which is in a good agreement with the above agarose gel electrophoresis (Figure 3). The easiness of dissociation of the polyplexes strongly correlates with the total transgene expression in vitro as shown in Figure 2. However, these results do not necessarily indicate the polyplex disassembly in the cells before the transcription. It is also possible that the polyplexes are directly recognized by the transcription factors without the disassembly. When the luciferase activities in in vitro system for p(DMAPAA46-*co*-MPC53-*co*-SA1) (1.0×10^5 RLU) and p(DMAPAA40-*co*-MPC60) (0.7×10^5 RLU) in the absence of PVSK (see above) were compared, the direct transcription was also improved slightly by adding just 1% of stearyl group in the linear polycation. The micelle-type amphiphilic carriers were able to improve the intracellular transcription via both of these mechanisms.

It was found that DNA complexing with the copolymers having stearyl residues is much more easily replaced with added PVSK than the case of the linear-type copolymers (Figure 3). The amphiphilic copolymers were found to form micelle-like structure. These carriers promote the transcription caused by easiness of DNA release from the polyplexes and by less entanglement. These results suggest that the factor of carrier topology is important to detemine the expression efficiency.

References and Notes

Present address: Department of Biomedical Engineering, Advanced Medical Engineering Center, National Cardiovascular Center Research Institute, 5-7-1 Fujishirodai, Suita, Osaka 565-8565

1 S. C. De Smedt, J. Demeester, and W. E. Hennink, *Pharm. Res.*, **17**, 113 (2000).

2 C. Kneuer, M. Sameti, U. Bakowsky, T. Schiestel, H. Schirra, H. Schmidt, and C. M. Lehr, *Bioconjugate Chem.*, **11**, 926 (2000).

3 J. H. Jeong, S. H. Song, D. W. Lim, H. Lee, and T. G. Park, *J. Controlled Release*, **73**, 391 (2001).

4 G. Y. Wu and C. H. Wu, *Biochemistry*, **27**, 887 (1988).

5 O. Boussif, F. Lezoualc'h, M. A. Zanta, M. D. Mergny, D. Scherman, B. Demeneix, and J. P. Behr, *Proc. Natl. Acad. Sci.*, **92**, 7297 (1995).

6 C. K. Chan and D. A. Jans, *Hum. Gene Ther.*, **10**, 1695 (1999).

7 T. Yamaoka, T. Kimura, R. Iwase, and A. Murakami, *Macromol. Biosci.*, **2**, 437 (2002).

8 I. Lee and K. Akiyoshi, *Biomaterials*, **25**, 2911 (2004).

9 J. K. Lam, Y. Ma, S. P. Armes, A. L. Lewis, T. Baldwin, and S. Stolnik, *J. Controlled Release*, **100**, 293 (2004).

10 M. Licciardi, Y. Tang, N. C. Billingham, S. P. Armes, and A. L. Lewis, *Biomacromol.*, **6**, 1085 (2005).

11 S. Katayose and K. Kataoka, *Bioconjugate Chem.*, **8**, 702 (1997).

12 P. Erbacher, A. C. Roche, M. Monsigny, and P. Midoux, *Bioconjugate Chem.*, **6**, 401 (1995). A mixture of 50 μL of polyplex suspension and 50 μL of chloroquine solution (200 μM) was added to monolayer culture of 1.0×10^4 seeded cells in a single well of a 96-well multiplate, incubated for 8 h, and then cultured in a fresh medium for another 40 h. Luciferase activity of the cell lysate in Trion-X100 solution was measured on a Lumicounter ATP-300 (ADVANTEC MFS, INC., USA).

13 T. Yamaoka, H. Iwata, N. Hamada, H. Ide, and Y. Kimura, *Nucleic Acids Symp. Ser.*, **31**, 229 (1994).

Published on the web (Advance View) September 28, 2005; DOI 10.1246/cl.2005.1478

Nucleic Acids Symposium Series No. 49 365–366

The destabilization of polyplexes facilitates intranuclear transcription efficiency

Tomoko Hashimoto[1,2], Akio Kobori[2] Akira Murakami[2] and Tetsuji Yamaoka[1]

[1]Department of Biomedical Engineering, National Cardiovascular Center Research Institute, Fujishirodai, Suita, Osaka 565-8585, Japan and [2]Department of Polymer Science and Engineering, Kyoto Institute of Technology, Matsugasaki, Sakyo-ku, Kyoto 606-8585,Japan

ABSTRACT

We have been focusing on the last step of transfection, that is, the intranuclear recognition of polyplexes by transcription factors. In this work, we studied about the relationship between the intracellular destabilization of polyplexes and the transcription efficiency. Polypeptides containing specific sequences which are digested by intracellular proprotein convertase(PC), furin(Fur-polypeptide) were synthesized as novel carriers. When Fur-polypeptide/plasmid DNA polyplexes were incubated with furin in the cell-free transcription/translation system, the sequence specific expression was observed as time. Additionally, Fur-polypeptides/plasmid DNA polyplexes led to site-specific effective transgene expression even in COS-1 cells. These results indicate that shortened carriers lose their abilities to form polyplexes in response to furin activity in the cells, and it seems to enhance the destabilization of polyplexes, the recognition of transgene in polyplexes by transcription factors, and the expression efficiency.

INTRODUCTION

In non-viral carrier mediated gene therapy, various intracellular mechanisms of polymeric carrier/gene polyplexes have been gradually clarified. The conventional evaluation of these polyplexes mediated gene delivery systems shows the total efficiency including all steps, such as cellular uptakes, endosomal escapes, nuclear transfers, and intranuclear expressions of transgene.

We have been focusing on the last step following the intracellular barriers described above, transcription of transgene. Since the transcription efficiency seems to be affected by condensation of the polyplex, optimum molecular design of polymeric gene carriers for high transcription efficiency should be clarified. Generally, linear polycations such as poly(L-lysine) (PLL) are known as DNA condensers. In order to relax the condensation between polymeric carrier and transgene, we have designed various polymeric gene carriers that are cationic polymers conjugated with hydrophilic or hydrophobic segments. Some PLL derivatives showed that quanternary ammonium groups and non-ionic hydrophilic groups led to high transfection efficiency[1]. On the other hand, cationic copolymers with hydrophobic segment formed micelle-like structure in aqueous solution and improved the expression efficiency because of an easy disassembly of polyplexes and recognition of the DNA in polyplexes.

These results indicated that both of the reciprocal factors, hydrophilic and hydrophobic, commonly destabilize electrostatic polyplexes and facilitate transgene expressions. Following these factors, a biological factor was proposed in the present study. Polypeptide containing sequences recognized and cleaved by intracellular proprotein convertase(PC), furin(Fur-polypeptide) was selected as a novel destabilization carrier. This intracellular enzymatic digestion-induced destabilization of polyplexes led to site-specific transgene expression[2]. In the present study, we evaluated whether these enhanced expression efficiencies were brought by high transcription efficiencies or not.

RESULTS AND DISCUSSION

Since furin digests the carboxyl side of Arg-Xaa-Xaa-Arg[3], H_2N-(Arg-Lys-Arg-Lys-Lys-Arg)$_4$-Cys-$CONH_2$ and H_2N-(Arg-Lys-Arg-Lys-Arg-Lys)$_4$-Cys-$CONH_2$ were synthesized as a digestible and control carrier, and they were abbreviated as Fur-3 and Fur-4, respectively. These polypeptides are highly cationic enough to form polyplexes with plasmid DNA. Digestion assay with furin were conducted by a modified method of previously reported one[2] using Fur-polypeptide/pT7-Luc polyplexes(C/A=5) at a fixed concentration of human recombinant furin convertase(Affinity BioReagents, Inc., USA). The destabilization of polyplexes was observed on the ethidium bromide stained agarose gel(0.8%) electrophoresis. We selected *in vitro* transcription/translation assay as the cell-free evaluation system of the transcription efficiency. The polyplex was evaluated using T_NT Coupled Reticulocyte

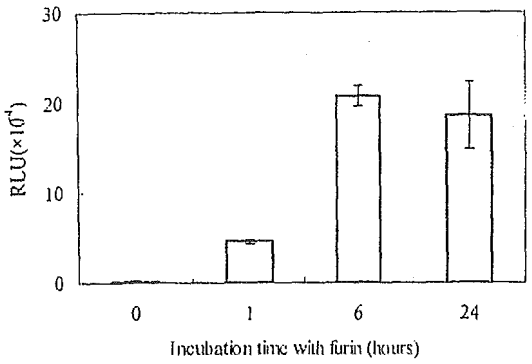

Figure 1. Transcription efficiency determined by luciferase activity *in vitro* transcription/translation system. Fur-3/pT7-Luc polyplexes(C/A=5) were digested with 5units of furin for a given period of time and used.

Lysate Systems(Promega, USA). Polyplexes composed of Fur-polypeptide were destabilized chronologically. In case of Fur-3, the DNA release from destabilized polyplexes was observed clearly, and transcription efficiency of digested polyplexes in the cell-free system were increased time-dependently (Figure 1.). Especially polyplexes reacted with furin for 6hours resulted in a about 100-fold enhancement compared with non-reacted polyplexes. It was reported that low molecular weight carriers easily release DNA under intracellular environment[4]. These results indicate that furin digestion resulted in the loss of the polyplex forming ability of the carriers, the destabilization of polyplexes, and higher transcription efficiency. These enhancements indicate that the enzymatic-destabilization actually occurs in the intracellular compartments when Fur-polypeptide is used as a gene carrier.

To assess the intracellular transcription efficiencies, the osmotic shock procedure and the microinjection were selected as transfection protocols. PLL and its derivatives having quaternary ammonium groups and non-ionic hydrophilic groups were used as carriers. To quantify the transcription efficiency of transgene in single cell, Cy3-labeled pCMV-Luc and pEGFP-N1 were transfected at optimum ratio into COS-1 cells by the osmotic shock method. The fluorescence intensity of Cy3(585nm) and EGEP(520nm) were measured on the FACS system with a 488nm excitation laser 40h after the onset of transfection to assess the cellular uptake and transient expression. The transcription efficiency is defined as following equation (1).

$$\text{Transcription efficiency in single cell} = \frac{\text{Fluorescence intensity of expressed EGFP}}{\text{Fluorescence intensity of uptaked Cy3}} \quad (1)$$

Although PLL and all derivatives showed similar degree of nuclear transfer of plasmid DNA(data not shown), only PLL derivative having quaternary ammonium groups and hydroxy groups showed high transcription. These results indicate that polyplexes formed with these chemical structures also play an important role to destabilize the polyplexes during the intracellular trafficking.

In conclusion, the polyplex destabilization was induced by the enzymatic fragmentation and the chemically modified characterization, and they facilitate their transcription efficiencies.

REFERENCES

1. Kimura, T., Yamaoka, T., Iwase, R., and Murakami, A. (2002) *Macromol. Biosci.* **2**, 437-446
2. Hashimoto, T., Murakami, A. and Yamaoka, T., (2004) *Nucleic Acids Res Suppl.*, **48**, 235-236.
3. Hosaka, M., Nagahama, M., Kim, W. S., Watanabe, T., Hatsuzawa, K., Ikemizu, J., Murakami, K., and Nakayama, K. (1991) *J. Biol. Chem.* **266**, 12127-12130
4. Schaffer, D. V., Fidelman, N. A., Dan, N., and Lauffenburger, D. A. (2000) *Biotechnol. Bioeng.* **67**. 598-606